

e^+e^- pairs from π^-A reactions *

Th. Weidmann, E. L. Bratkovskaya, W. Cassing, and U. Mosel

Institut für Theoretische Physik, Universität Giessen

D-35392 Giessen, Germany

Abstract

We present a dynamical study of e^+e^- production in π^-A reactions at 1.3 and 1.7 GeV on the basis of the Coupled-Channel-BUU approach. The contributions from vector mesons (ρ, ω) are calculated taking into account the collisional broadening effect and are compared to background sources in the dilepton spectrum from πN bremsstrahlung as well as the Dalitz decays of ω and η mesons produced in the reaction. Two possible scenarios for the medium modifications of the vector mesons are investigated, i.e. the dropping mass scheme for the ρ and ω and a momentum dependent ρ -meson spectral function that includes the polarization of the ρ -meson due to resonant $\rho - N$ scattering.

PACS: 25.80.-e, 25.80.Hp

Keywords: leptons, pion induced reactions

*Work supported by BMBF and GSI Darmstadt.

I. INTRODUCTION

The properties of hadrons in the nuclear medium are of fundamental interest (cf. Refs. [1–5]). According to QCD sum rules [4–6] or QCD inspired effective Lagrangian models [1–3,7–12,?] the properties of the vector mesons (ρ , ω and ϕ) should change with the nuclear density. Furthermore, along with a dropping mass the phase space for the resonance decay also decreases which results in a modification of the resonance lifetime in matter. On the other hand, due to collisional broadening – which depends on the nuclear density and the resonance-nucleon interaction cross section (cf. Refs. [14,15]) – the resonance lifetime decreases again.

The in-medium properties of vector mesons have been studied experimentally so far by dilepton measurements at SPS energies for proton-nucleus and nucleus-nucleus collisions [16–19]. As proposed by Li *et al.* [20,21], the observed enhancement in A + A reactions compared to p + A collisions in the invariant mass range $0.3 \leq M \leq 0.7$ GeV might be due to a shift of the ρ -meson mass following Brown/Rho scaling [1] or the Hatsuda and Lee sum rule prediction [4]. The microscopic transport studies in Refs. [22–24] for these systems support these results [20,21].

However, also a more conventional approach including the change of the ρ -meson spectral function in the medium due to the coupling of ρ , π , Δ and nucleon dynamics along the lines of Refs. [7–10] was found to be (roughly) compatible with the CERES data [10,22]. Meanwhile, our knowledge on the ρ spectral function has improved since – as first pointed out by Friman and Pirner [11] – resonant ρ -N interactions significantly enhance the strength in the vector-isovector channel at low invariant mass; this has also been confirmed recently in Ref. [13] where the authors find a significant smearing of the ρ strength at low ρ momenta due to a selfconsistent evaluation of the resonance widths. In fact, the CERES data for S + Au at 200 A GeV and Pb + Au at 160 A GeV, using an expanding fireball model, were found to be compatible with such a hadronic scenario [12].

Recently, the thermodynamical result of Ref. [12] was supported by HSD transport cal-

culations [25] where an improved ρ spectral function was used. The conclusion in Ref. [25] was that both the 'dropping mass' scenario [21–24] as well as the hadronic spectral function approach [12] lead to dilepton spectra which are in good agreement with the experimental data for all systems at SPS energies. A similar analysis was done also for BEVALAC/SIS energies [26] (where quite different temperature and density regimes are probed) involving both the spectral functions from Refs. [12,13]. It was found that these spectral functions give practically the same result for dilepton spectra at BEVALAC/SIS energies.

Additional, and possibly more sensitive, information could be provided by studies using more elementary probes such as pions or protons as incoming particles. In such reactions the nuclear density ($\leq \rho_0$) is obviously lower than in heavy-ion collisions, but the phase-space distribution of the nuclear matter is almost stationary and much better known. In the case of pion-nucleus reactions the ω meson can be produced with low momenta in the laboratory system such that a substantial fraction of them will also decay inside a heavy nucleus [27–29]. In Refs. [28,29], which employed the Hatsuda-Lee mass shift [4], it was shown on the basis of the intranuclear cascade (INC) approach that the mass distributions of the vector mesons decaying inside the nucleus have a two-component structure [15] in the dilepton invariant mass spectrum: the first, high-mass component corresponds to resonances decaying in the vacuum, thus showing the free spectral function which is very narrow in case of the ω meson; the second (broader) component of lower masses corresponds to the resonance decay inside the nucleus.

The many detailed hadronic model studies quoted above have shown that the assumption of a very narrow, unchanged width of the vector mesons, that underline the Hatsuda-Lee prescription, is oversimplified. This has also recently been discussed in Ref. [6], where the authors have shown that QCD sum rules pose only very loose constraints on the in-medium properties of vector mesons.

In this paper we, therefore, report results of detailed microscopic calculations on the basis of the CBUU model for the dilepton production in π^-C , π^-Ca , π^-Pb collisions at kinetic energies $E_{kin} = 1.3$ and 1.7 GeV employing also realistic spectral function [13] in

addition to the collisional broadening and 'dropping' mass effects of vector mesons studied in Refs. [28,29].

Our paper is organized as follows: In Section 2 we briefly describe the CBUU transport approach and its implementation for pion-induced reactions, the πN total reaction cross section and the elementary processes for meson production and their interactions employed in the CBUU. In Section 3 we discuss the elementary channels for dilepton production and collisional broadening and the in-medium modification schemes ('dropping' mass and ρ spectral function approach) which will be applied for calculating the dilepton spectra. Section 4 contains a detailed study of dilepton spectra for π^-C , π^-Ca , π^-Pb reactions at $E_{kin} = 1.3$ and 1.7 GeV. We close with a summary in Section 5.

II. INGREDIENTS OF THE CBUU-MODEL

A. Binding energy and nuclear stability

The dynamical description of pion-nucleus collisions is performed within the Coupled-Channel-BUU (CBUU) approach [30] which has been found to describe reasonably well various pion data at SIS energies. The model has been described in detail in [30]; here we briefly recall the main ingredients.

In line with Refs. [31–34] the dynamical evolution of heavy-ion collisions or hadron-nucleus reactions below the pion-production threshold is described by a transport equation for the nucleon one-body phase-space distribution function $f_N(\vec{r}, \vec{p}, t)$,

$$\begin{aligned} \frac{\partial f(\vec{r}, \vec{p}, t)}{\partial t} + \left\{ \frac{\vec{p}}{E} + \frac{m^*(\vec{r}, \vec{p})}{E} \vec{\nabla}_p U(\vec{r}, \vec{p}) \right\} \vec{\nabla}_r f(\vec{r}, \vec{p}, t) \\ + \left\{ -\frac{m^*(\vec{r}, \vec{p})}{E} \vec{\nabla}_r U(\vec{r}, \vec{p}) \right\} \vec{\nabla}_r f(\vec{r}, \vec{p}, t) = I_{coll}[f(\vec{r}, \vec{p}, t)], \end{aligned} \quad (1)$$

where \vec{r} and \vec{p} denote the spatial and the momentum coordinate of the nucleon, respectively, while N stands for a proton (p) or neutron (n). The effective mass $m^*(\vec{r}, \vec{p})$ in Eq. (1) includes the nucleon restmass $m_N (= 938 \text{ MeV}/c^2)$ as well as a scalar momentum-dependent mean-field potential $U(\vec{r}, \vec{p})$,

$$m^*(\vec{r}, \vec{p}) = m_N + U(\vec{r}, \vec{p}) \quad (2)$$

for the baryons. The nucleon quasi-particle dispersion relation then is

$$E(\vec{r}, \vec{p}) = \sqrt{m^*(\vec{r}, \vec{p})^2 + \vec{p}^2}. \quad (3)$$

In the CBUU-model we explicitly propagate the mesonic degrees of freedom π , η , ρ and a scalar meson σ that simulates correlated 2π pairs in the isospin 0-channel. Besides the nucleon and the $\Delta(1232)$ we, furthermore, include all baryonic resonances up to a mass of 1950 MeV/ c^2 : i.e. $N(1440)$, $N(1520)$, $N(1535)$, $\Delta(1600)$, $\Delta(1620)$, $N(1650)$, $\Delta(1675)$, $N(1680)$, $\Delta(1700)$, $N(1720)$, $\Delta(1905)$, $\Delta(1910)$ and $\Delta(1950)$, the resonance properties are adopted from the PDG [35].

Denoting the nucleon by N and the baryon resonances listed above by R and R' , we include explicitly the following channels:

- elastic baryon-baryon collisions $NN \leftrightarrow NN, NR \leftrightarrow NR$;
- inelastic baryon-baryon collisions $NN \leftrightarrow NR, NR \leftrightarrow NR', NN \leftrightarrow \Delta(1232)\Delta(1232)$;
- inelastic baryon-meson reactions $R \leftrightarrow N\pi, R \leftrightarrow N\pi\pi, \Delta(1232)\pi, N(1440)\pi, N\rho, N\sigma$;
 $N(1535) \leftrightarrow N\eta; NN \leftrightarrow NN\pi$;
- meson-meson collisions $\rho \leftrightarrow \pi\pi$ (p-wave), $\sigma \leftrightarrow \pi\pi$ (s-wave)

Particles propagating inside nuclear matter are exposed to the mean-field potential generated by all other particles. Here we employ the momentum-dependent mean-field potential proposed by Welke et al. [36] with an additional isospin symmetry potential U^{symm} , i.e.

$$U^{nr}(\vec{r}, \vec{p}) = A\frac{\rho}{\rho_0} + B\frac{\rho^\tau}{\rho_0} + 2\frac{C}{\rho_0} \int d^3p' \frac{f(\vec{r}, \vec{p}')}{1 + \left(\frac{\vec{p}-\vec{p}'}{\Lambda}\right)^2} + U^{symm}, \quad (4)$$

where U^{symm} is

$$U^{symm} = D\frac{\rho_p(\vec{r}) - \rho_n(\vec{r})}{\rho_0}\tau_z, \quad (5)$$

$\tau_z = -1$ for neutrons and $\tau_z = +1$ for protons; for the strength of the symmetry potential we use $D = 30$ MeV in line with [37].

As an extension of the momentum-independent Skyrme type potentials for nuclear matter [33,36] the parametrization (4) has no manifest Lorentz-properties. However, definite Lorentz-properties are required for a transport model at relativistic energies. To achieve this goal we evaluate the non-relativistic mean-field potential U^{nr} in the local rest frame (LRF) of nuclear matter which is defined by the frame of reference with vanishing local vector baryon current ($\vec{j}(r, t) = \vec{0}$). Assuming only scalar potentials in the LRF we then equate the expressions for the single-particle energies using the non-relativistic potential U^{nr} and the scalar potential U by

$$\sqrt{p^2 + m^2} + U^{nr}(\vec{r}, \vec{p}) = \sqrt{p^2 + (m + U(\vec{r}, \vec{p}))^2}. \quad (6)$$

Eq. (6) now allows to extract the scalar mean-field potential $U(\vec{r}, \vec{p})$ which we will use throughout our calculations for the baryons.

For our calculations we use a (momentum-dependent) equation of state (EOS) for nuclear matter with an incompressibility of $K = 290$ MeV (i.e. $A = -29.3$ MeV, $B = 57.2$ MeV, $C = -63.5$ MeV, $\tau = 1.760$, $\Lambda = 2.13$ fm $^{-1}$.)

Since we investigate collisions of pions with nuclei it is important that the nuclear ground state properties, i.e. density and binding energies, are well reproduced. We illustrate the quality of our ground state in Fig. 1, where we show the binding energy per nucleon as a function of the nucleon number A . The solid curve corresponds to the binding energy calculated with U^{symm} whereas the dashed curve is the result without the isospin symmetry potential; the solid curve belongs to nuclei that are quite stable over time periods longer than the typical reaction time of 15 fm/c in case of a Pb-target. Comparing our calculations for stationary nuclei with the empirical liquid drop result (dotted line) we find that our dynamical calculations with U^{symm} agree reasonably well with the experimental systematics.

B. πN total reaction cross sections

In order to describe pion-baryon scattering in the framework of the resonance picture a Breit-Wigner formulation for the cross sections (eq. $\pi N \rightarrow mN$) was used

$$\sigma_{ab \rightarrow R \rightarrow cd} = \frac{2J_R + 1}{(2S_a + 1)(2S_b + 1)} \frac{4\pi}{p_i^2} \frac{s \Gamma_{R \rightarrow ab} \Gamma_{R \rightarrow cd}}{(s - M_R^2)^2 + s \Gamma_{tot}^2}. \quad (7)$$

In Eq. (7) ab and cd denote the baryon and the meson in the initial and final state of the reaction and R is the intermediate baryon resonance. J_R , S_a and S_b are the spins of the baryon resonance and the particles in the initial state of the reaction, while $\Gamma_{R \rightarrow ab}$, $\Gamma_{R \rightarrow cd}$ are taken from the PDG [35] and p_i^2 stands for the squared momentum of the incoming meson in the resonance rest frame.

The solid line in Fig. 2 shows the total $\pi^- - p$ -cross section within the CBUU model in comparison to the experimental data from [38]. To calculate this cross section we replace the partial widths $\Gamma_{R \rightarrow cd}$ in Eq. (7) by the total widths of the baryonic resonances and sum up the contributions from all resonances. The dot-dot-dashed, the dot-dashed and the short-dashed lines in Fig. 2 show the contributions from the $\Delta(1232)$, the $N(1440)$ and the $N(1520)$ separately. We supplement the resonances included in Ref. [30] with an additional effective two-pion production channel (long-dashed line) in order to reproduce properly the total cross section data at high $s^{1/2}$ which is quite essential for $\pi+A$ reactions in the energy regime considered here. By using instead of this scheme an effective resonance with a one-pion decay width we have ascertained that our results are independent of the specific way in which the missing pion strength at high energies is corrected.

C. Elementary processes for meson production and meson-baryon interactions

Because of the small cross sections involved we can treat the production of vector mesons (ρ, ω) and η 's perturbatively. Since we work within the parallel ensemble algorithm, each parallel run of the transport calculation can be considered approximately as an individual reaction event, where binary reactions in the entrance channel at given invariant energy

\sqrt{s} lead to final states with 2 or 3 particles with a relative weight W_i for each event i . W_i is defined by the ratio of the production cross section to the total hadron-hadron cross section¹. The perturbative treatment implies that the initial hadrons are not modified in their respective final channels. On the other hand, each perturbative particle is represented by a testparticle with weight W_i and propagated according to the Hamilton equations of motion. Elastic and inelastic reactions with baryons are computed in the standard way [39]. The final cross section is obtained by multiplying each testparticle with its weight W_i . In this way one achieves a time-saving simulation of the vector meson production, propagation and reabsorption during the pion-nucleus collision.

The η mesons are produced in pion-baryon and baryon-baryon collisions according to the elementary production cross sections from Ref. [40,41]. However, in the present analysis we assume the $pn \rightarrow pn\eta$ cross section to be about 6 times larger than the $pp \rightarrow pp\eta$ cross section close to threshold in line with the new data from the WASA collaboration [42].

For the vector mesons (ρ, ω) we have to take into account the pion-baryon production channels $\pi^-p \rightarrow \omega n, \pi^-N \rightarrow \omega X, \pi^-p \rightarrow \rho n, \pi^-N \rightarrow \rho X$ and in addition to [28,29] the baryon-baryon channels $BB \rightarrow \rho BB, BB \rightarrow \rho X, BB \rightarrow \omega BB, BB \rightarrow \omega X$.

For the exclusive process $\pi^-p \rightarrow \omega n$ we use a parametrization of the experimental data from Ref. [43]:

$$\sigma_{\pi^-p \rightarrow \omega n}^{excl.} = C \frac{p_{\pi N} - p_{\omega}^0}{p_{\pi N}^{\alpha} - d}, \quad (8)$$

where $p_{\pi N}$ is the relative momentum (in GeV/c) of the pion-nucleon pair while $p_{\omega}^0 = 1.095$ GeV/c is the threshold value. The parameters $C = 13.76$ mb (GeV/c) $^{\alpha-1}$, $\alpha=3.33$ and $d=1.07$ (GeV/c) $^{\alpha}$ describe satisfactorily the data on the energy-dependent cross section in the near-threshold energy region. For ρ^0 -meson production $\pi^-p \rightarrow \rho n$ we use the same cross section as for the ω -meson; this holds experimentally within 20%.

¹The actual final states are chosen by Monte Carlo sampling according to the 2 or 3-body phase space.

For the inclusive vector meson production $\pi^- p \rightarrow VX$, $V = \omega, \rho$ we use the parametrization from Ref. [45]

$$\sigma_{\pi^- p \rightarrow VX}^{incl.} = a_V (x-1)_V^b x^{-c_V}, \quad (9)$$

where the scaling variable is defined as $x = s/s_{th}$, $s_{th} = m_N + m_V$. For ω -production we have $a_\omega = 4.8$ mb, $b_\omega = 1.47$, $c_\omega = 1.26$; for ρ -production we have $a_\rho = 3.6$ mb, $b_\rho = 1.47$, $c_\rho = 1.26$.

For the vector meson production in baryon-baryon channels (this contribution is quite small for $\pi^- A$ reactions) we also use the parametrization from Ref. [45]

$$\sigma_{pp \rightarrow VX}^{incl.} = a_V (x-1)_V^b x^{-c_V}, \quad (10)$$

where the scaling variable is defined again as $x = s/s_{th}$, $s_{th} = 2m_N + m_V$. For ω -production we use $a_\omega = 2.2$ mb, $b_\omega = 1.47$, $c_\omega = 1.1$; for ρ -production we use $a_\rho = 2.5$ mb, $b_\rho = 1.47$, $c_\rho = 1.11$.

For the interactions of vector mesons with baryons we include the following channels: $\omega N \rightarrow \omega N$, $\omega N \rightarrow \pi N$, $\omega N \rightarrow \pi\pi N$; $\rho N \rightarrow \rho N$, $\rho N \rightarrow \pi N$, $\rho N \rightarrow \pi\pi N$. For these reactions no experimental data are directly available and we adopt the parametrizations from Ref. [28,29]. The total ωN cross section is described as

$$\sigma_{\omega N}^{tot}(p_{lab}) = A + \frac{B}{p_{lab}} \quad (11)$$

with $A = 11$ mb and $B = 9$ mb GeV/c. The elastic ωN cross section is parametrized as

$$\sigma_{\omega N}^{el}(p_{lab}) = A \frac{1}{1 + a p_{lab}} \quad (12)$$

with $A = 20$ mb and $a = 1$ GeV⁻¹c.

For the ρ -N total and elastic cross sections we adopt the results of Ref. [44], which were calculated within the resonance model using the experimental branching ratios for the resonances involved [35]:

$$\begin{aligned} \sigma_{\rho^0 N}^{tot} &= 26.0 + 0.9 \lambda^{-3}(s, m_N, m_\rho) \text{ [mb]} \\ \sigma_{\rho^0 N}^{el} &= 13.0 + 0.25 \lambda^{-3}(s, m_N, m_\rho) \text{ [mb]}, \end{aligned} \quad (13)$$

where $\lambda(z, x, y) = [z - (x + y)^2] \cdot [z - (x - y)^2]$.

The channel $\rho N \rightarrow \pi N$ is determined via detailed balance from the inverse reaction (8) whereas the ω absorption channel is described by $\sigma_{\omega N}^{abs} = \sigma_{\omega N}^{tot} - \sigma_{\omega N}^{el}$.

In order to demonstrate the relevant range of the elementary production cross sections we display in Fig. 3 the distribution in the pion-baryon collision number versus the invariant energy \sqrt{s} above the threshold for ρ production $\sqrt{s_{th}} = m_N + m_\rho$, i.e. $dN/d\sqrt{s}$ (histogram) for π^- Pb at $E_{kin} = 1.3$ GeV. The arrow indicates the incoming energy. Due to Fermi motion and secondary interactions the $dN/d\sqrt{s}$ is not a sharp peak, but a broader distribution.

III. DILEPTON PRODUCTION

A. Elementary channels

The dilepton production is calculated perturbatively by including the contributions from the Dalitz-decays $\Delta \rightarrow Nl^+l^-$, $N(1440) \rightarrow Nl^+l^-$, $N(1520) \rightarrow Nl^+l^-$, $N(1535) \rightarrow Nl^+l^-$, $\pi^0 \rightarrow \gamma l^+l^-$, $\eta \rightarrow \gamma l^+l^-$, $\omega \rightarrow \pi^0 l^+l^-$ and the direct dilepton decays of the vector mesons ρ and ω , where the ρ meson may as well be produced in $\pi^+\pi^-$ collisions. For a detailed description of the Δ, N^* Dalitz decays we refer the reader to Ref. [40]; the dilepton decays of the η and vector mesons are described in Ref. [24].

The novel channel included as compared to Refs. [28,29] is the Dalitz decay of the $N(1520)$ resonance which is described in the same way as the Δ resonance with spin 3/2 (see [40]), but using a coupling constant $g = 0.96$ and $\Gamma_0 = 1.1$ MeV in Eqs. (4.8)-(4.13) in Ref. [40].

B. In-medium vector mesons and collisional broadening

1. Collisional broadening

Following [28,29] we assume that (in first order) the in-medium resonance can also be described by a Breit-Wigner formula with a mass and width distorted by the nuclear envi-

ronment:

$$F(M) = \frac{1}{2\pi} \frac{\Gamma_V^*}{(M - m_V^*)^2 + \Gamma_V^{*2}/4} \quad (14)$$

containing the effects of collisional broadening,

$$\Gamma_V^* = \Gamma_V + \delta\Gamma, \quad (15)$$

where

$$\delta\Gamma = \gamma v \sigma_{VN}^{tot} \rho_N, \quad (16)$$

as well as a shift of the meson mass

$$m_R^* = m_V + \delta m_V. \quad (17)$$

In Eq. (16) v is the resonance velocity with respect to the target at rest, γ is the associated Lorentz factor, ρ_N is the nuclear density and σ_{VN}^{tot} is the meson-nucleon total cross section. For $\sigma_{\rho N}^{tot}$ we use Eq. (13) while for $\sigma_{\omega N}^{tot}$ we adopt Eq. (11). In using (15) we neglect the decrease in the width due to the lowered mass of the vector mesons, which is small compared to the collisional broadening.

In Fig. 4 we show the width of ρ and ω mesons calculated dynamically according to Eqs. (15),(16) (open squares) for π^- Pb at $E_{kin} = 1.3$ GeV. The solid lines indicate a linear fit of the form

$$\Gamma_V^*(\rho_N) = \Gamma_V^0(\rho_N) \left(1 + \beta \frac{\rho_N}{\rho_0} \right), \quad (18)$$

where $\beta = 1.55$ for the ρ -meson and $\beta = 9$ for the ω -meson. While the collisional broadening is roughly twice that of the bare ρ -width, it increases the width of the ω -meson by about one order of magnitude.

2. 'Dropping' vector meson mass

In order to explore the observable consequences of vector meson mass shifts at finite nuclear density the in-medium vector meson masses are modelled according to Hatsuda and Lee [4] or Brown/Rho scaling [1] as

$$m_V^* = m_V(1 - \alpha\rho_N(r)/\rho_0), \quad (19)$$

where $\rho_N(r)$ is the nuclear density at the resonance decay, $\rho_0 = 0.16 fm^{-3}$ and $\alpha = 0.18$ for the ρ and ω .

3. The ρ spectral function

As discussed earlier the simple mass shift is a simplified approximation. For the ρ -meson we therefore also include a calculated spectral function [13]. The implementation of the ρ spectral function into the transport approach for the calculation of the dilepton yield from ρ^0 decay is described in detail in Refs. [25,26]. Here we adopt the same strategy, i.e. the dilepton radiation from ρ mesons in the vector dominance model is calculated as

$$\frac{dN_{\rho \rightarrow l^+l^-}}{dM} = -\frac{2M}{\pi} \text{Im}D_\rho(q_0, q; \rho_N), \quad (20)$$

where D_ρ is the ρ -meson propagator [13] in the hadronic medium depending on the baryon density ρ_N as well as on energy q_0 and 3-momentum $q \equiv |\vec{q}|$ in the local rest frame of the baryon current ('comoving' frame). The invariant mass M is related to the ρ -meson 4-momentum in the nuclear medium as $M^2 = q_0^2 - q^2$, while $\text{Im}D_\rho$ is spin averaged over the longitudinal and transverse part of the ρ -propagator [13].

IV. DILEPTONS FROM π A REACTIONS

In Fig. 5 we present the calculated dilepton invariant mass spectra $d\sigma/dM$ for π^- Pb at the bombarding energy of $E_{kin} = 1.3$ GeV. The upper part corresponds to the result calculated without collisional broadening and free meson masses. The middle part shows the dilepton spectra calculated including the collisional broadening effect and 'dropping' masses of ρ and ω mesons (Eq. (19)), whereas the lower part corresponds to calculations with collisional broadening, a mass shift for the ω -meson and the momentum and density-dependent ρ spectral function [13] (Eq. (20)) instead of a 'dropping' ρ -mass. The thin lines

indicate the individual contributions from the different production channels; *i.e.* starting from low M : Dalitz decay $\eta \rightarrow \gamma e^+ e^-$ (dotted line), $\Delta \rightarrow N e^+ e^-$ (short-dotted line), $\omega \rightarrow \pi^0 e^+ e^-$ (dot-dashed line), $N(1520) \rightarrow N e^+ e^-$ (dot-dashed line), $N(1535) \rightarrow N e^+ e^-$ (long-dashed line), proton-neutron bremsstrahlung (dashed line), πN bremsstrahlung (short-dashed line); for $M \approx 0.8$ GeV: $\omega \rightarrow e^+ e^-$ (dashed line), $\rho^0 \rightarrow e^+ e^-$ (dot-dashed line). The full solid line represents the sum of all sources. The dominant background processes are the pion-nucleon bremsstrahlung, calculated in the soft-photon approximation which might be considered as an upper limit, and also the η and ω Dalitz decays. The contributions from heavy-baryon resonances are negligibly small. Above $M \sim 0.6$ GeV the spectrum is dominated by the vector meson decays with a low background from other hadronic sources.

As seen from the middle part, the mass shift and the collisional broadening effect leads to a two-component structure for the ω meson: the narrow peak at $M = m_\omega$ comes from the ω decaying outside the nucleus whereas the broader peak corresponds to the decay inside the nucleus. For the ρ meson this effect is not seen because the ρ mesons practically all decay inside the nucleus due to their short lifetime, only the width of the ρ meson peak becomes larger due to collisional broadening. The 'dropping' mass for the ρ and ω mesons leads to an essential reduction of the vector meson production threshold in meson-baryon and baryon-baryon collisions and to a slight enhancement of vector meson production in pion-nucleus collisions. A similar effect is seen if one employs the ρ spectral function (lower part in Fig. 5) instead of a dropping ρ -mass.

We have also performed similar calculations for light systems (in order to test different density regimes) and two incoming energies. In Figs. 6,7 we show the dilepton invariant mass spectra $d\sigma/dM$ for π^-C , π^-Ca and π^-Pb at the bombarding energies of $E_{kin} = 1.3$ and 1.7 GeV, respectively. The solid lines indicate the sum of all dilepton channels calculated without collisional broadening and with free meson masses. The dotted lines are the results with collisional broadening and a 'dropping' mass of ρ and ω mesons. The dashed lines correspond to calculations with collisional broadening, with dropping ω mass and with the ρ spectral function [13]. The dropping mass scheme leads to an enhancement by about a

factor 2 as compared to the free meson mass in the dilepton range $0.6 \leq M \leq 0.7$ GeV and to a reduction by about a factor 2 above the ω peak. The ρ spectral function also slightly enhances the yield at $0.6 \leq M \leq 0.7$ GeV, however, the reduction above the ω peak is not so strong as compared to the free meson mass case. As seen from Figs. 6,7 the difference between the three scenarios exists even for a light system like ^{12}C and becomes more pronounced for heavy nuclei (^{208}Pb) due to the larger volume.

In Fig. 8 we present the same analysis as in Fig. 7, but the dilepton spectra were calculated including a cut in the longitudinal momentum of the dileptons, i.e. $q_z \leq 0.3$ GeV/c, which makes the differences between the dropping mass scheme and the ρ spectral function more pronounced. Fig. 8 demonstrates that with a proper q_z cut one should be able to distinguish experimentally between the two scenarios for the medium modifications of the vector mesons.

In Fig. 9 we show the transverse momentum distribution for $\pi^- \text{C}$, $\pi^- \text{Ca}$ and $\pi^- \text{Pb}$ at the bombarding energy of $E_{kin} = 1.7$ GeV integrated over all invariant masses. The assignment is the same as in Fig. 6. The dominant contributions come from pion-nucleon bremsstrahlung at $M \leq 0.4$ GeV and from the η Dalitz decay for $M \geq 0.4$ GeV due to the larger cross section in comparison to the other dilepton sources (see Fig. 5). The measurement of the transverse momentum spectra integrated over all M might provide an additional check of the theoretical models especially for the πN bremsstrahlung calculation. Applying an invariant mass cut $0.6 \leq M \leq 1.0$ GeV allows to separate the vector meson contributions from the background sources.

V. SUMMARY

On the basis of the Coupled-Channel-BUU approach we have studied dilepton production in $\pi^- \text{C}$, $\pi^- \text{Ca}$ and $\pi^- \text{Pb}$ collisions at $E_{kin} = 1.3$ and 1.7 GeV. Various contributions are taken into account for dilepton production: the Dalitz-decays of Δ , $N(1440)$, $N(1520)$, $N(1535)$ resonances and η , ω mesons, proton-neutron bremsstrahlung, πN bremsstrahlung as well as

the direct dilepton decays of the vector mesons ρ and ω .

The contributions from vector mesons were calculated including the collisional broadening and by applying two different in-medium modification schemes of the vector mesons: i) the dropping mass and ii) the hadronic spectral function approach [13].

It was found that both scenarios lead to similar results – an enhancement of the dilepton yield at $0.6 \leq M \leq 0.77$ GeV and a depletion above the ω -resonance. However, these models predict different absolute values for the dilepton yield at invariant masses below and above $M = m_V$. This difference can be studied experimentally especially after applying proper longitudinal momentum cuts.

ACKNOWLEDGMENTS

The authors are grateful for various discussions with H. Bokemeyer, Ye.S. Golubeva, W. Koenig, L.A. Kondratyuk, W. Kühn, V. Metag, W. Schön and A. Sibirtsev. Furthermore, they are indebted to M. Post and W. Peters for the ρ spectral function from Ref. [13] prior to publication.

REFERENCES

- [1] G.E. Brown and M. Rho, Phys. Rev. Lett. 66 (1991) 2720.
- [2] C.M. Shakin and W.-D. Sun, Phys. Rev. C 49 (1994) 1185.
- [3] F. Klingl and W. Weise, Nucl. Phys. A 606 (1996) 329; F. Klingl, N. Kaiser and W. Weise, hep-ph/9704398.
- [4] T. Hatsuda and S. Lee, Phys. Rev. C 46 (1992) R34.
- [5] M. Asakawa and C.M. Ko, Phys. Rev. C 48 (1993) R526.
- [6] S. Leupold, W. Peters and U. Mosel, nucl-th/9708016.
- [7] M. Herrmann, B. Friman, and W. Nörenberg, Nucl. Phys. A560 (1993) 411.
- [8] M. Asakawa, C. M. Ko, P. Lévai, and X. J. Qiu, Phys. Rev. C46 (1992) R1159.
- [9] G. Chanfray and P. Schuck, Nucl. Phys. A545 (1992) 271c.
- [10] R. Rapp, G. Chanfray, and J. Wambach, Phys. Rev. Lett. 76 (1996) 368.
- [11] B. Friman and H. J. Pirner, Nucl. Phys. A617 (1997) 496.
- [12] R. Rapp, G. Chanfray and J. Wambach, Nucl. Phys. A617 (1997) 472.
- [13] W. Peters, M. Post, H. Lenske, S. Leupold, and U. Mosel, nucl-th/9708004.
- [14] L. A. Kondratyuk, M. Krivoruchenko, N. Bianchi, E. De Sanctis and V. Muccifora, Nucl. Phys. A 579 (1994) 453.
- [15] K.G. Boreskov, J. Koch, L.A. Kondratyuk and M.I. Krivoruchenko, Phys. of Atomic Nuclei 59 (1996) 1908.
- [16] G. Agakichiev et al., Phys. Rev. Lett. 75 (1995) 1272.
- [17] Th. Ullrich et al., Nucl. Phys. A610 (1996) 317c; A. Drees, Nucl. Phys. A610 (1996) 536c.

- [18] M. A. Mazzoni, Nucl. Phys. A566 (1994) 95c; M. Masera, Nucl. Phys. A590 (1995) 93c.
- [19] T. Åkesson et al., Z. Phys. C68 (1995) 47.
- [20] G. Q. Li, C. M. Ko, and G. E. Brown, Phys. Rev. Lett. 75 (1995) 4007.
- [21] C. M. Ko, G. Q. Li, G. E. Brown, and H. Sorge, Nucl. Phys. A610 (1996) 342c.
- [22] W. Cassing, W. Ehehalt, and C. M. Ko, Phys. Lett. B363 (1995) 35.
- [23] W. Cassing, W. Ehehalt, and I. Kralik, Phys. Lett. B377 (1996) 5.
- [24] E. L. Bratkovskaya and W. Cassing, Nucl. Phys. A619 (1997) 413.
- [25] W. Cassing, E. L. Bratkovskaya, R. Rapp, and J. Wambach, nucl-th/9708020, Phys. Rev. C (1997) in press.
- [26] E. L. Bratkovskaya, W. Cassing, R. Rapp, and J. Wambach, nucl-th/9710043.
- [27] W. Schön, H. Bokemeyer, W. Koenig, and V. Metag, Acta Physica Polonica B27 (1996) 2959.
- [28] W. Cassing, Ye.S. Golubeva, A.S. Iljinov, and L.A. Kondratyuk, Phys. Lett. B 396 (1997) 26.
- [29] Ye.S. Golubeva, L.A. Kondratyuk and W. Cassing, nucl-th/9710071, Nucl. Phys. A (1997), in press.
- [30] S. Teis, W. Cassing, M. Effenberger, A. Hombach, U. Mosel, and Gy. Wolf, Z. Phys. A 356 (1997) 421; Z. Phys. A 359 (1997) in press.
- [31] G. F. Bertsch and S. Das Gupta, Phys. Rep. 160 (1988) 189.
- [32] W. Cassing, K. Niita and S. J. Wang, Z. Phys. A 331 (1988) 439.
- [33] W. Cassing, V. Metag, U. Mosel and K. Niita, Phys. Rep. 188 (1990) 363.
- [34] K. Weber, B. Blättel, W. Cassing, H.-C. Dönges, V. Koch, A. Lang and U. Mosel, Nucl.

- Phys. A 539 (1992) 713; K. Weber, B. Blättel, W. Cassing, H.-C. Dönges, A. Lang, T. Maruyama and U. Mosel, Nucl. Phys. A 552 (1993) 571.
- [35] Review of Particle Properties: Phys. Rev. D 50 (1994).
- [36] G. Welke, M. Prakash, T.T.S. Kuo and S. Das Gupta, Phys. Rev. C 38 (1988) 2101.
- [37] B.A. Li, Z.Z. Ren, C.M. Ko, and S.Y. Yennello, Phys. Rev. Lett. 76 (1996) 4492.
- [38] Baldini et al., *Landolt-Börnstein* vol. 12, Springer, Berlin (1987)
- [39] W. Cassing and U. Mosel, Prog. Part. Nucl. Phys. 25 (1990) 235.
- [40] Gy. Wolf, G. Batko, W. Cassing, U. Mosel, K. Niita, and M. Schäfer, Nucl. Phys. A 517 (1990) 615; Gy. Wolf, W. Cassing and U. Mosel, Nucl. Phys. A 552 (1993) 549.
- [41] T. Vetter, A. Engel, T. Biro and U. Mosel, Phys. Lett. B 263 (1991) 153.
- [42] WASA collaboration, preliminary data.
- [43] J. Cugnon, P. Deneye and J. Vandermeulen, Phys. Rev. C 41 (1990) 1339.
- [44] A. Sibirtsev and W. Cassing, preprint UGI-97-20, Nucl. Phys. A (1997), in press.
- [45] A. Sibirtsev, W. Cassing and U. Mosel, Z. Phys. A 358 (1997) 357.

FIGURES

FIG. 1. The binding energy per nucleon as a function of the nucleus mass number. The solid curve corresponds to the binding energy calculated with the symmetry potential U^{symm} whereas the dashed curve is the result of a calculation without U^{symm} . The dotted line corresponds to the empirical values.

FIG. 2. The calculated total $\pi^- - p$ -cross section in comparison to the data from [38] (solid line). The dot-dot-dashed, the dot-dashed and the short-dashed lines show the contributions from the $\Delta(1232)$, the $N(1440)$ and the $N(1520)$ separately. The long-dashed line indicates the contribution of the additional two pion production channel.

FIG. 3. The distribution in the pion-baryon collision number versus the invariant energy \sqrt{s} above the threshold for ρ production $\sqrt{s_0} = m_N + m_\rho$, i.e. $dN/d\sqrt{s}$ (histogram), for π^- Pb at $E_{kin} = 1.3$ GeV. The arrow indicates the incoming energy.

FIG. 4. The width of the ρ and ω mesons calculated according to Eqs. (15),(16) (open squares) for π^- Pb at $E_{kin} = 1.3$ GeV. The solid lines indicate a linear fit with density according to Eq. (18).

FIG. 5. The dilepton invariant mass spectra $d\sigma/dM$ for π^- Pb at the bombarding energy of $E_{kin} = 1.3$ GeV calculated without collisional broadening and with free meson masses (upper part), including the collisional broadening effect and a 'dropping' mass of the ρ and ω mesons (middle part) as well as including the ρ spectral function from Ref. [13] instead of a 'dropping' ρ -mass (lower part). The thin lines indicate the individual contributions from the different production channels; *i.e.* starting from low M : Dalitz decay $\eta \rightarrow \gamma e^+ e^-$ (dotted line), $\Delta \rightarrow N e^+ e^-$ (short-dotted line), $\omega \rightarrow \pi^0 e^+ e^-$ (dot-dashed line), $N(1520) \rightarrow N e^+ e^-$ (dot-dashed line), $N(1535) \rightarrow N e^+ e^-$ (long-dashed line), proton-neutron bremsstrahlung (dashed line), πN bremsstrahlung (short-dashed line); for $M \approx 0.8$ GeV: $\omega \rightarrow e^+ e^-$ (dashed line), $\rho^0 \rightarrow e^+ e^-$ (dot-dashed line). The full solid line represents the sum of all sources.

FIG. 6. The dilepton invariant mass spectra $d\sigma/dM$ for π^-C , π^-Ca and π^-Pb at the bombarding energy of $E_{kin} = 1.3$ GeV. The solid lines indicate the sum of all dilepton channel calculated without collisional broadening and with free meson masses. The dotted curves are the result with collisional broadening and 'dropping' masses of ρ and ω mesons. The dashed curves correspond to the calculations with collisional broadening, dropping ω mass and with the ρ spectral function from Ref. [13].

FIG. 7. The dilepton invariant mass spectra $d\sigma/dM$ for π^-C , π^-Ca and π^-Pb at the bombarding energy of $E_{kin} = 1.7$ GeV. The assignment is the same as in Fig. 6.

FIG. 8. The dilepton invariant mass spectra $d\sigma/dM$ for π^-C , π^-Ca and π^-Pb at the bombarding energy of $E_{kin} = 1.7$ GeV with a longitudinal momentum cut $q_z \leq 0.3$ GeV/c. The assignment is the same as in Fig. 6.

FIG. 9. The transverse momentum distribution for π^-C , π^-Ca and π^-Pb at the bombarding energy of $E_{kin} = 1.7$ GeV integrated over all invariant masses. The assignment is the same as in Fig. 6.

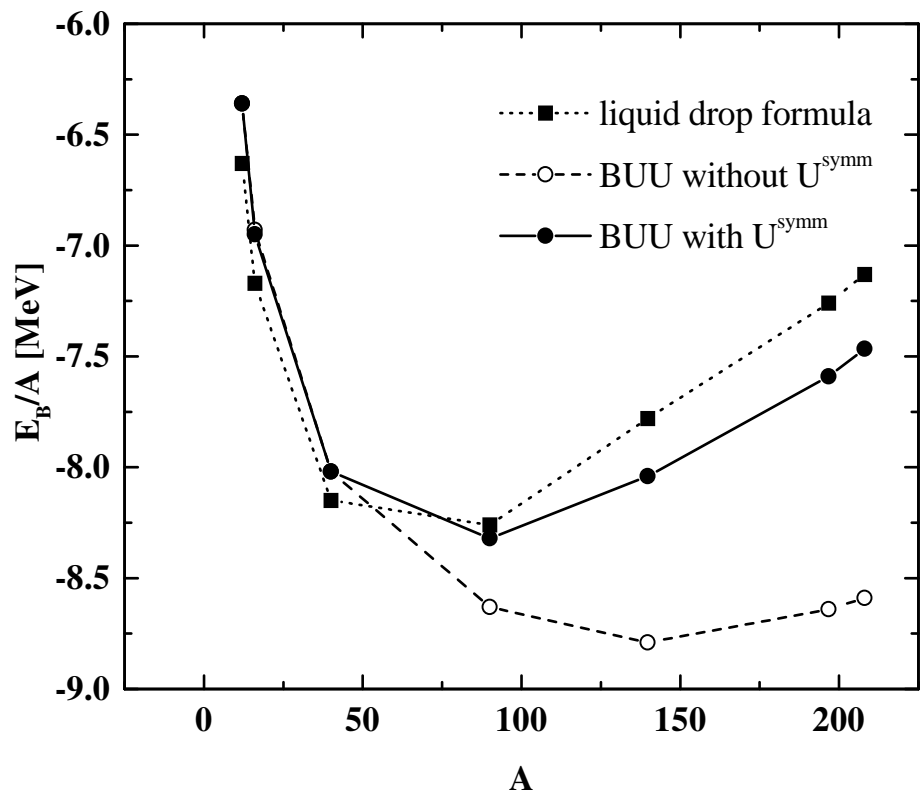


Fig. 1

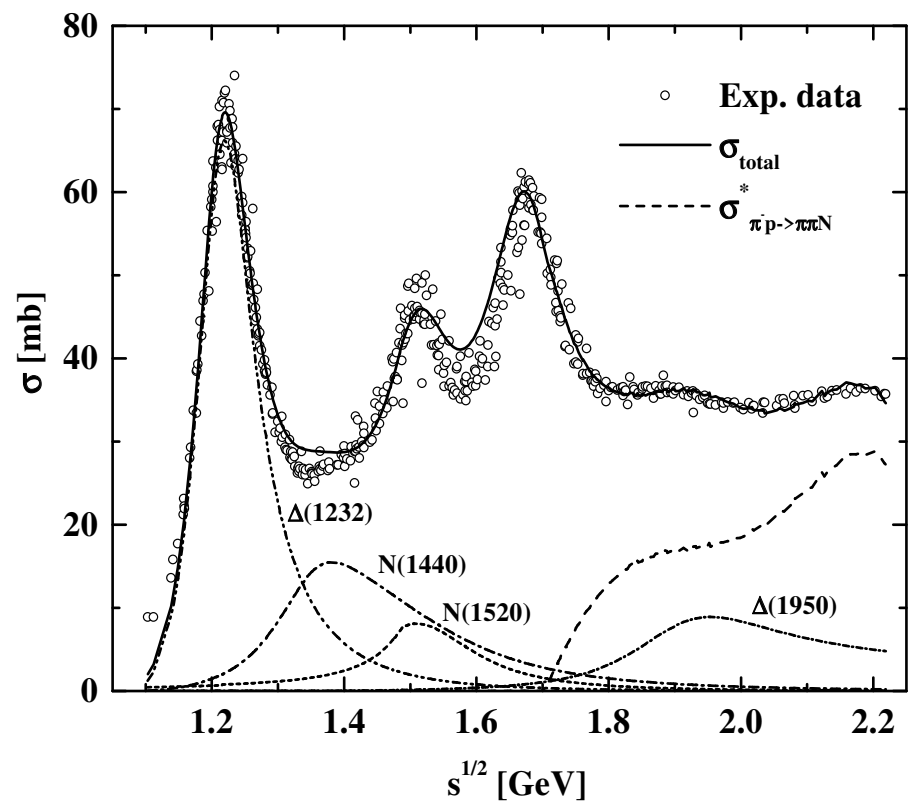


Fig. 2

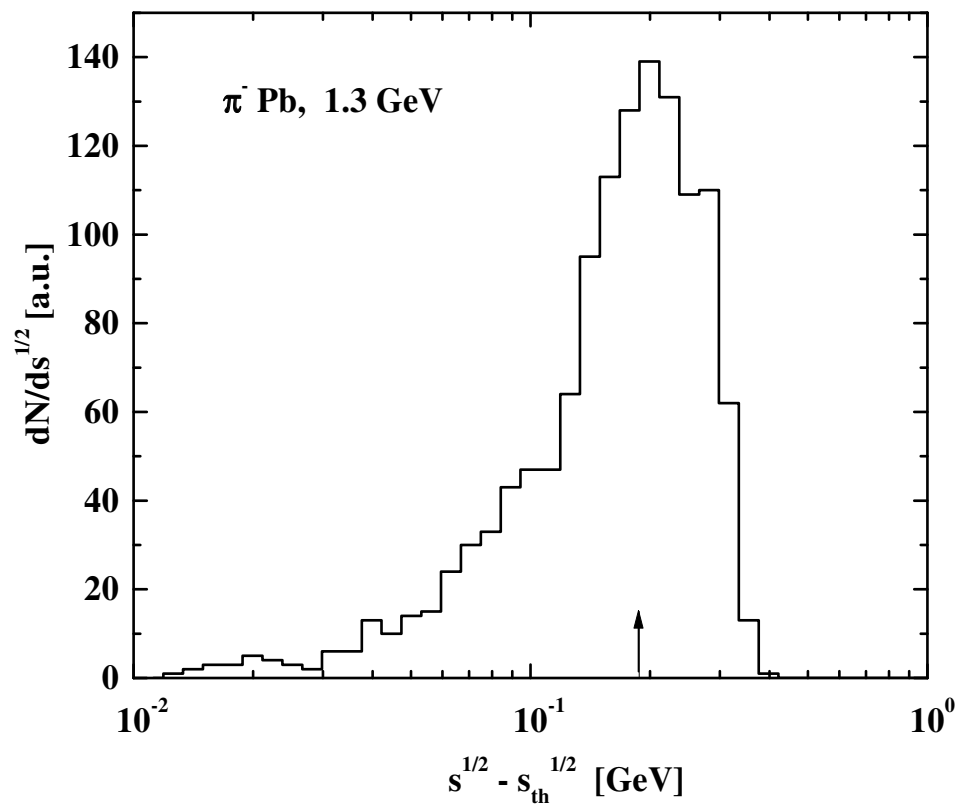


Fig. 3

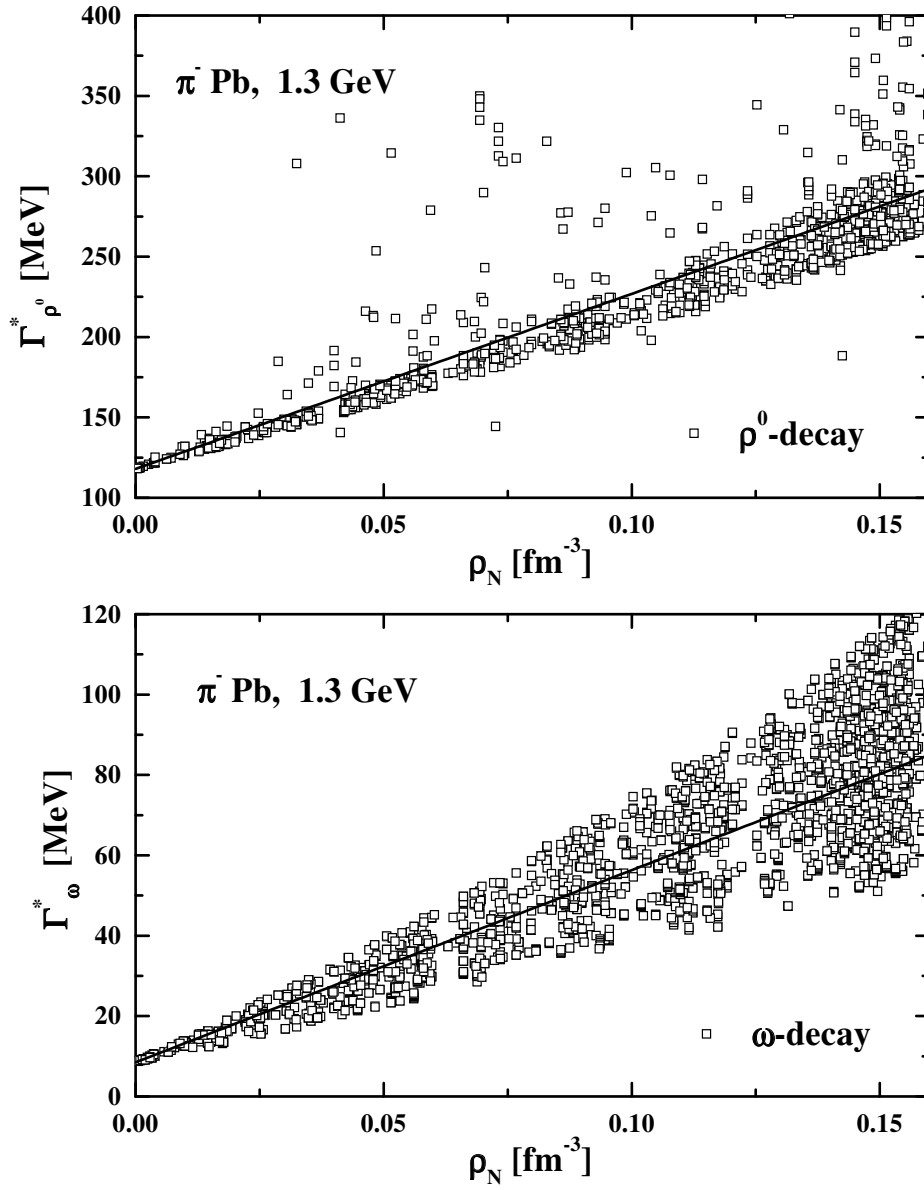


Fig. 4

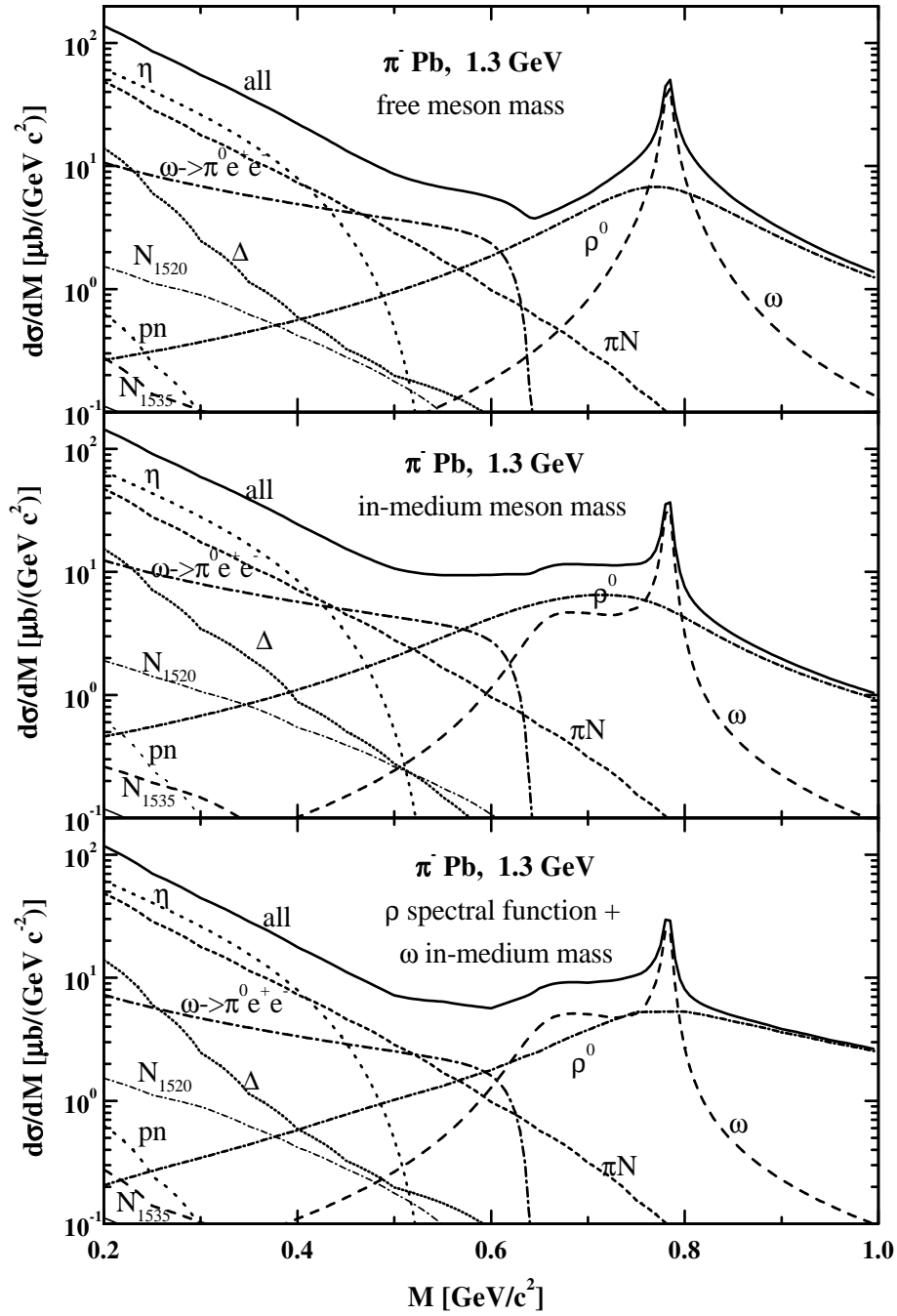


Fig. 5

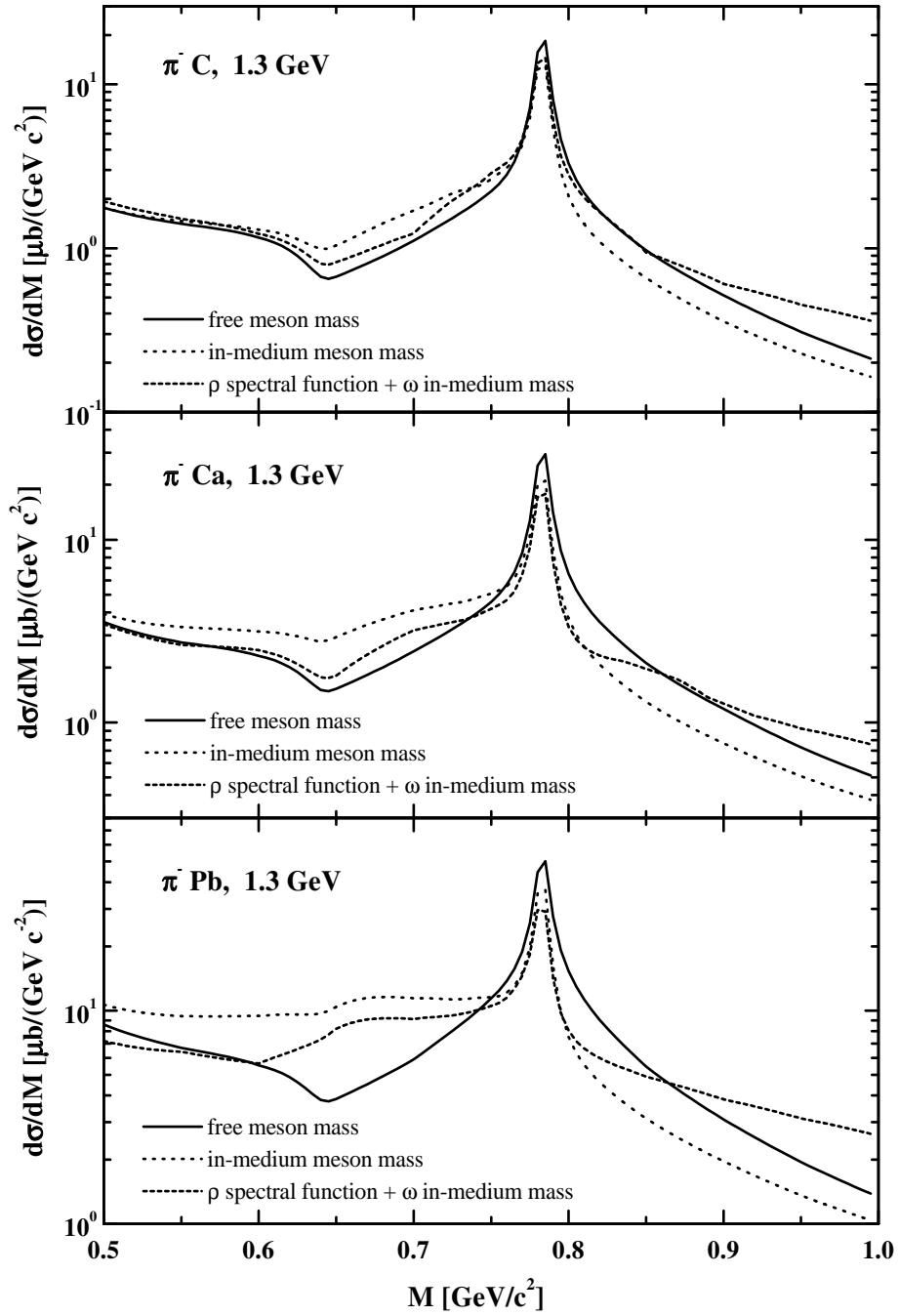


Fig. 6

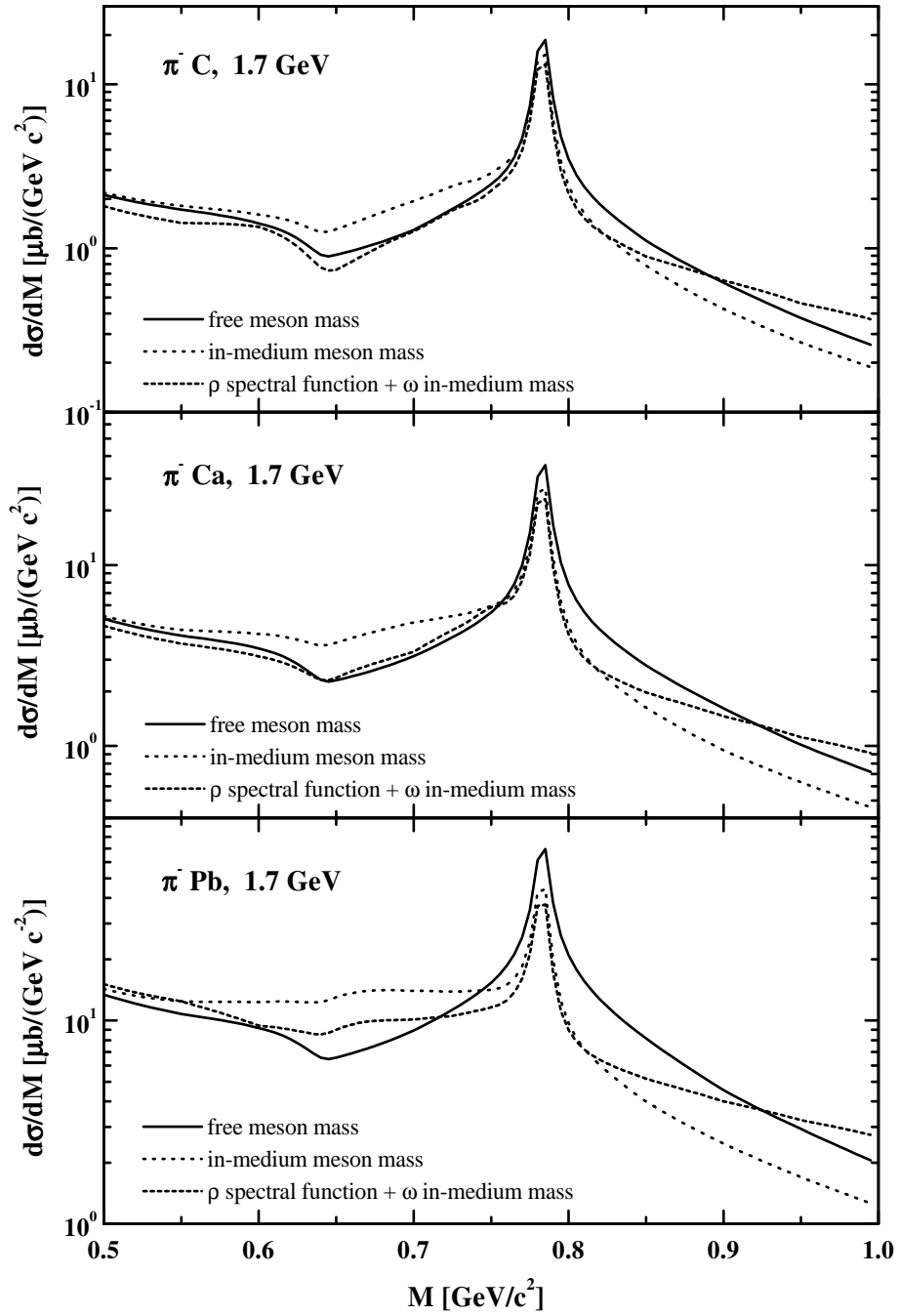


Fig. 7

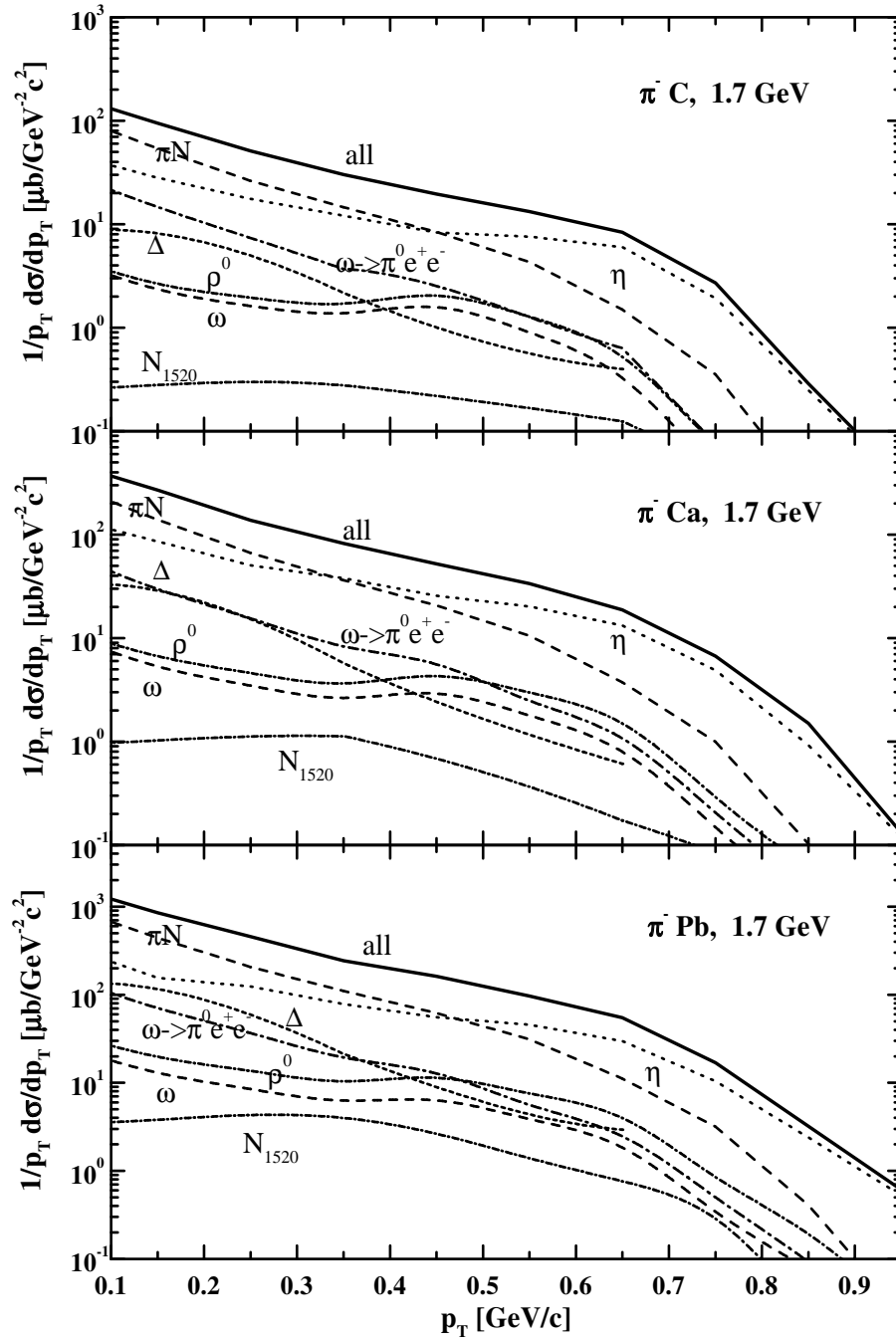


Fig. 9

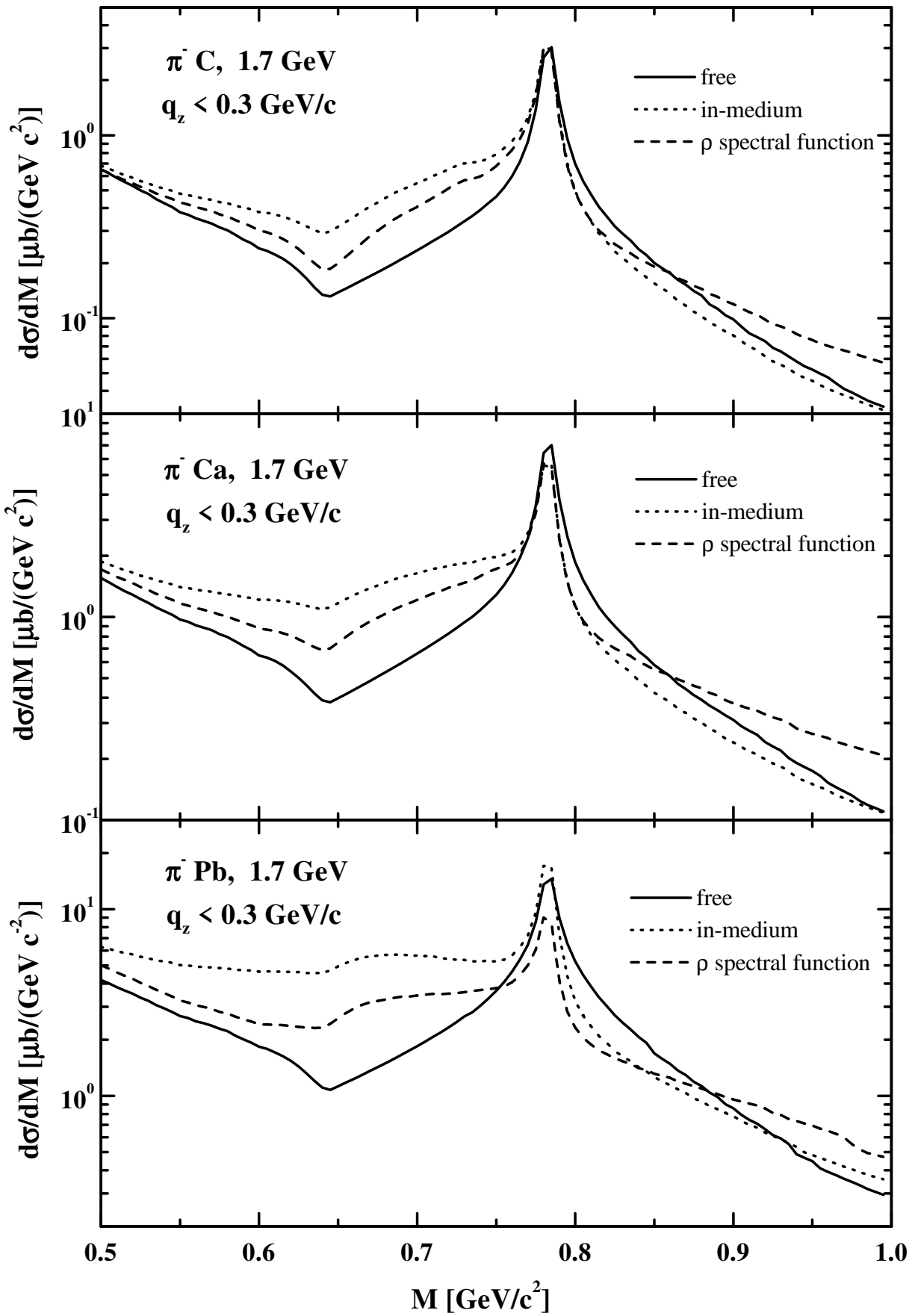


Fig. 8

